IMPROVING THE ASSISTED BIDIRECTIONAL GLENN DESIGN FOR BETTER EJECTOR PUMP EFFECT AND LOWER SVC PRESSURE

A Thesis

Presented to the Faculty of the Graduate School

of Cornell University

In Partial Fulfillment of the Requirements for the Degree of

Master of Science

by

Dongjie Jia

May 2020

ABSTRACT

The assisted bidirectional Glenn (ABG) procedure was proposed to address the drawbacks of the modified Blalock-Taussig shunt (mBTS) and the bidirectional Glenn (BGD) procedures, as an alternative to first and second stage palliation for neonates with single-ventricle physiology. This thesis introduces a modified ABG (mABG) design to address previous ABG drawbacks of high SVC pressure. The performances are compared with realistic 3-dimensional multiscale simulations. Two simulation methods developed to improve accuracy and reduce costs are introduced: an adaptive mesh refinement method and an aortic pressure regulatory method. A parametric optimization study shows that the optimal nozzle area is around 16% of the SVC cross-sectional area, the optimal nozzle width and the optimal shunt diameter are both 3.5 mm. Simulations show the mABG was able to preserve all advantages of the original ABG procedure while reducing the SVC pressure to 4.3 mmHg at normal PVR. There is no significant improvement in the SVC pressure for high PVR, motivating more extensive paramedic studies.

BIOGRAPHICAL SKETCH

Dongjie (Fred) Jia, B.Sc., is a graduate student in mechanical engineering at Cornell University. His research interest focuses on computational fluid dynamics and cardiovascular engineering. Dongjie graduated from Rensselaer Polytechnic Institute with a B.Sc. in mechanical engineering in 2018. His undergraduate research focused on using CFD to predict left atrium hydrodynamical changes for patients undergoing surgical left atrial appendage closure. The study was awarded first place in the 2018 Rensselaer Polytechnic Institute Undergraduate Research Symposium. The manuscript is published in Cardiovascular Engineering and Technology. During his M.S. program, Dongjie focused on modifying the assisted bidirectional Glenn procedure for better performance, as well as developing modeling techniques for cardiovascular simulations. The work is presented in this thesis.

ACKNOWLEDGMENTS

I would like to thank Professor Mahdi Esmaily for the guidance and help throughout this study. His inputs and knowledge not only helped push this project forward but also helped me develop as a professional. I would like to thank Dr. Tigran Khalapyan for the inputs and discussions during this study. His clinical insights are very valuable. I would like to thank Professor James Antaki for the contribution and help in my M.S. exam. I would like to also thank Dr. Viktor Hraska and Dr. Alexander Opotowsky for their comments.

I would like to thank Matthew Peroni for the hard work in running parts of the simulations. I would like to thank Grant Rydquist and Chenwei (Andy) Meng for the helps and suggestions during the development of the simulation algorithms.

TABLE OF CONTENTS

LIST OF FIGURES

LIST OF TABLES

LIST OF ABBREVIATIONS

ABG – assisted bidirectional Glenn

mABG – modified assisted bidirectional Glenn

BA – brachiocephalic artery

BDG – bidirectional Glenn

mBTS – modified Blalock-Taussig shunt

BTS – Blalock-Taussig shunt

CFD – computational fluid dynamics

DILV – double inlet left ventricle

HLHS – hypoplastic left heart syndrome

IA – innominate artery

LBV – left brachiocephalic vein

LPN – lumped parameter network

MUPFES – multi-physics finite-element solver

PA – pulmonary artery

PID – proportional–integral–derivative

PVR – pulmonary vascular resistance

RBV – right brachiocephalic vein

SVC – superior vena cava

LIST OF SYMBOLS

A, cross-sectional area of veins or arteries
C, capacitor values
C_n, cardiac cycles
CO, cardiac output
e, PID controller error
E, finite element method error
EP_{eff}, ejector pump efficiency
h, mesh element edge length
HL, workload on the single ventricle
K_p, proportional gain
K_i, integral gain
K_d, derivative gain
OD, systemic oxygen delivery
OD_{cor}, coronary oxygen delivery
P, pressure
P_{ao}, aortic average pressure
P_{SVC}, superior vena cava average pressure
P_{PA}, pulmonary artery average pressure
PP_{PA}, pulmonary artery average pulse pressure
PI_{PA}, pulmonary artery average pulsatility index
PV, process variable
Q_P, pulmonary average flow rate
Q_S, systemic average flow rate
Q_{lb}, lower-body average flow rate
Q_{ub}, upper-body average flow rate
Q_{cor}, coronary average flow rate
r, adaptive mesh error tolerance
Sat_{ao}, aortic percentage oxygen saturation
SP, setpoint
u, velocity vector (adaptive mesh)
u, correction term (PID controller)
V, velocity magnitude
Vol, total blood volume

CHAPTER 1

CURRENT STATE OF SINGLE VENTRICLE BIRTH DEFECT TREATMENTS

Single ventricle birth defect (univentricular heart) occurs in approximately 5 cases for every 10,000 live births according to a New England regional report [1]. The most common types of single ventricle defects include hypoplastic left heart syndrome (HLHS), tricuspid atresia, and double inlet left ventricle (DILV) [2]. A three-stage procedure is required for patients with these complications. Right after birth, the first-stage palliation is performed commonly using a modified Blalock-Taussig shunt (mBTS) to establish a systemic-pulmonary flow. The single ventricle is responsible for both systemic and pulmonary flow as well as accepting both systemic and pulmonary returns. At around 6 months of age, the second stage bidirectional Glenn (BDG) procedure is performed. The stage-one shunt is removed and the superior vena cava (SVC) is connected directly to the pulmonary artery (PA). At this point, only the lower body flow returns to the single ventricle. The circulation schematics for the mBTS and the BDG procedures are shown in figure 1. The third stage procedure, namely the Fontan procedure, is performed after 18 months of age. The inferior vena cava is connected to the PA therefore completely separating the pulmonary circulation from the systemic circulation.

The overall mortality rate among patients with a single ventricle is as high as 29%[3], the majority of which occurred during the neonatal period of dependency on the systemic-pulmonary shunt, between stage-one mBTS and stage-two BDG procedures. The three leading causes for this adverse outcome are 1) insufficient oxygenation exacerbated by a flow imbalance between systemic and pulmonary circulation, 2) obstruction of pulmonary

circulation due to the shunt thrombosis, and 3) excessive workload on the single ventricle. These adverse effects were shown in a study of 122 postmortem cases where impairment of coronary arterial perfusion and excessive pulmonary flow (27% and 19% respectively) were found to be two major causes of death.[4] Also, the right vertical failure was reported in 13% of cases to be the cause of postoperative deaths, among which 68.5% was non-technical related.[4]

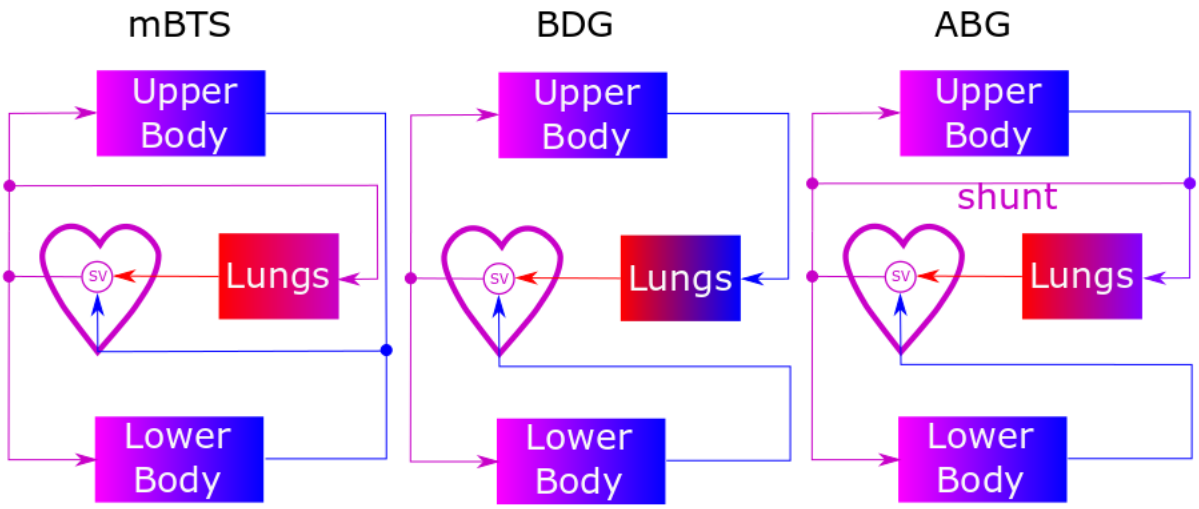

Figure 1. modified Blalock-Taussig shunt (mBTS), bidirectional Glenn (BDG), and assisted bidirectional Glenn (ABG) circulation schematics with colors showing oxygenation level. The color scheme represents the blood oxygen saturation level. SV, single ventricle.

Multiple attempts have been made to address challenges associated with the mBTS physiology. One of the initial attempts was to improve the systemic and coronary oxygen delivery of the mBTS circulation by optimizing the size and placement of the shunt using computational fluid dynamics (CFD) simulations.[5] The study found that a standard 3.5 mm shunt placed between innominate and pulmonary arteries is already optimal for an average newborn. Adding a second

shunt between the aorta and pulmonary artery (PA) to prevent total obstruction of pulmonary circulation in case of a shunt thrombosis also showed to be ineffective as it lowered oxygenation and created a thrombogenic region in the PA.[6] These two studies and those by others[7] confirmed that a standard mBTS physiology and its variants are fundamentally ineffective in aspects of high ventricle workload and low oxygen saturation.

Considering the drawbacks of the mBTS procedure, more recent studies proposed early BDG intervention up to 3 months of age.[8] The potential benefits include preserving ventricle and valve function by reducing single ventricle workload, as well as lowering risks of pulmonary diseases caused by the systemic-pulmonary shunt.[9] However, performing BDG at younger ages faces the challenge of low aortic oxygen saturation after the operation, which results in longer ICU stay. [8] Performing BDG at birth is further deemed impossible due to complications related to high pulmonary vascular resistance (PVR), such as SVC syndrome and cerebral damage.[10] These complications are likely caused by insufficient PA flow and high SVC pressure.

To overcome issues enumerated above, the assisted bidirectional Glenn (ABG) procedure was proposed as an alternative for stage-one palliation.[11] The ABG is constructed on top of the BDG by establishing a connection between the SVC and the PA and also a shunt between the innominate artery and the SVC. Similar to a previous attempt[12], the ABG relied on the ejector pump effect to lower the SVC pressure. As shown in Figure 2, an industrial ejector pump uses a high velocity that mixes with the low energy fluid to move the fluid downstream without elevating upstream pressure. Similarly, the underlying idea for the ABG was that the shunt flow

coming from the systemic side is at elevated pressure and has a higher energy content that can be transferred to the flow coming from the SVC to reduce its pressure. CFD simulations validated by in vitro experiments showed that the ABG offers multiple improvements over the conventional stage-one mBTS operation.[11], [13] It reduced the workload on the single ventricle by half while increasing oxygen saturation and delivery by approximately 10%. Additionally, the ABG can potentially lower the total number of open-chest surgeries from three to two by combining the first two operations. Despite these favorable outcomes, the ABG has at minimum one major shortcoming: excessive SVC pressure. The initial simulation and subsequent optimization of the ABG anatomy using idealized and patient-specific anatomies showed that the SVC pressure is 7.9 mm Hg at normal PVR and could be as high as 15 mm Hg at elevated PVR.[11], [14], [15] Such high pressure would lead to the development of venovenous collateral and may damage the developing brain.[16], [17]

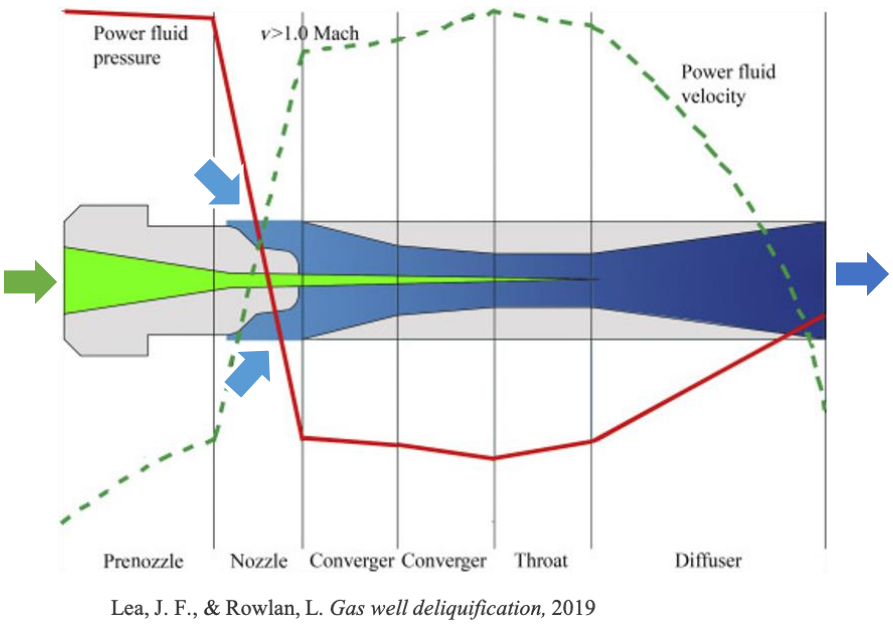

Figure 2. Ejector pump working schematics, as illustrated in [11, Fig. 3.41]. Power fluid marked in green and low energy fluid in blue.

This thesis presents a modified ABG design with reduced SVC pressure by fully realizing the ejector pump effect in the SVC. The effectiveness of the design is determined using computational fluid dynamics (CFD) simulations. Several simulation algorithms developed to improve the cost and the accuracy of the simulations are described in Chapter 2. The modified ABG circulation that significantly reduces the SVC pressure is introduced in Chapter 3. An optimization study is also performed on the geometrical parameters related to the proposed modifications, which is presented in Chapter 4.

CHAPTER 2

EFFICIENT NUMERICAL METHODS FOR MESH REFINEMENT AND AORTIC PRESSURE CONTROL

Introduction

Simulating the blood flow for cardiovascular systems with good accuracy and reasonable cost is extremely challenging due to the scale and complexity of the geometry. Same to the previous ABG paper[11], a multidimensional coupled approach is used for this study. The regions of major interest: the aorta, shunt, SVC, PA, etc., are modeled in 3-dimension and resolved with an inhouse CFD solver[19]–[21]. Other parts of the circulatory system are modeled with the lumped parameter network (LPN)[7] that models the flow with resistors, capacitors, and inductors (0-dimensional). This approach provides high result accuracy in the regions of interest and reduces computational cost in the whole circulation.

A couple of challenges remain for the simulation. Due to the geometries, in the 3-dimensional CFD model, some regions have high velocity and high shear flow which requires extremely fine mesh, while other regions could produce accurate results with relatively coarse mesh. For conventional meshing methods without knowing the flow result, the mesh most likely has uniform elements. And since the simulation error scales with the element edge length squared[22], the number of elements needs to increase by 4.75 times for the error to reduce by half. Therefore, using a uniform mesh will be extremely costly to obtain accurate results. This study implements an adaptive meshing method[23] that re-meshes the flow field based on

previous simulation results. Mesh density will be distributed accordingly which ensures result accuracy while conserving simulation cost.

Another challenge lies in modeling the long-term effect of the autoregulatory system of the human body. For different heart operations, although the dynamics of the circulatory system are different, the body maintains the same level of average aortic pressure in the long-term by adding or extracting fluid from the circulatory system.[24] The LPN system used in the simulation performs similarly: the average aortic pressure is adjusted by changing the total blood volume in the circulatory system. The total blood volume, Vol, is calculated from the LPN variables that representing pressures at different points in the circulatory system, x, and capacitor values, C, as defined in equation 1 below.

$$Vol = \sum_{i} C_i x_i \qquad [1]$$

Since the circulations for the mBTS, BDG, ABG, and mABG procedures are different, the total blood volume required to obtain the same average aortic pressure for each model is different. To find the total blood volume that results in the desired aortic average pressure, a control algorithm is introduced in this study. The performance of variants of this algorithm will be discussed.

Adaptive mesh method

The adaptive mesh method[23] aims to optimize element distribution based on the error calculated from previous simulation results. In general, the error, E, in finite element

calculations is related to the element edge length, h, and the second derivative of velocity, $\nabla^2\boldsymbol{u}$, as defined in equation 2.

$$E \propto h^2|\nabla^2\boldsymbol{u}| \quad [2]$$

For optimal mesh distribution, the error should be uniform across all nodes. Here we introduce a non-dimensional error tolerance, r, which would be decided by the user depending desired on computational cost. Smaller tolerance will result in finer mesh hence more computational cost. The initial simulation would be performed on a conventional uniform mesh. Form the result of the simulation, the desired edge length, h, for each node is calculated as in equation 3, where u_{typ} is the average velocity of the fluid field needed for unit consistency.

$$h = \sqrt{r \cdot \frac{|\boldsymbol{u}_{typ}|}{|\boldsymbol{u}''|}} \quad [3]$$

The mesh is then be re-meshed using Tetgen[25] with desired edge length information provided. In practice, the algorithm would need several iterations to reach the desired error tolerance. The tolerance for iteration *n* is calculated as equation 4, where *nitr* is the total number of iterations defined by the user. This method ensures a constant growth rate for the total number of elements.

$$r_n = r^{\frac{n}{nitr}} \quad [4]$$

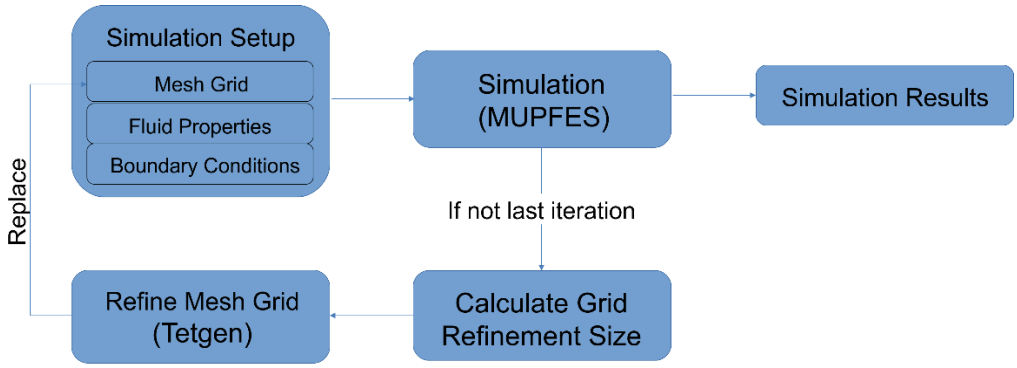

Figure 3. Workflow schematics of the adaptive mesh algorithm.

The adaptive mesh process is fully automated. For initialization, the user needs to provide the simulation parameter files the same as running a non-adaptive mesh case with the initial uniform mesh and its boundaries, as well as the number of processors available, number of iterations, and the error tolerance. The number of processors used for each iteration will be calculated based on the total number of elements but will not exceed the number of processors provided by the user. The commonly used number of iterations and tolerance level are 6 and 0.15, respectively. The overall workflow of the adaptive mesh algorithm is shown in figure 3. Currently, the algorithm is only compatible to be run on our lab's server with our in-house solver MUPFES.

To demonstrate the performance of the adaptive mesh method, three simulations of the same ejector pump design are performed on three different meshes: uniform coarse mesh, uniform fine mesh, and adaptive mesh, with 1 million, 10 million, and 2 million elements respectively. The nozzle upstream boundary has a constant pressure, the low-pressure upstream boundary has a constant flow rate, and the outlet boundary is set as a resistance boundary. The simulation run times are 2.7, 15.8, and 3.6 hours for the coarse mesh, fine mesh, and adaptive mesh,

respectively. The results of the three mesh methods are compared qualitatively in figure 4. An estimation for the simulation error can be calculated using the nozzle flow result of the coarse and fine mesh according to equation 1. The nozzle flow rates are 5.903 cm^3/s and 6.797 cm^3/s for the coarse and fine mesh respectively. The adaptive mesh resulted in a nozzle flow rate of 6.508 cm^3/s. Consider the fine mesh case to be the resulting benchmark, the coarse mesh resulting flow rate is 13.2% less than the result of the fine mech while the adaptive mesh resulting flow rate is only 4.2% off the fine mesh result. The adaptive mesh method lowers the difference by more than two-fold with little increase in computational cost.

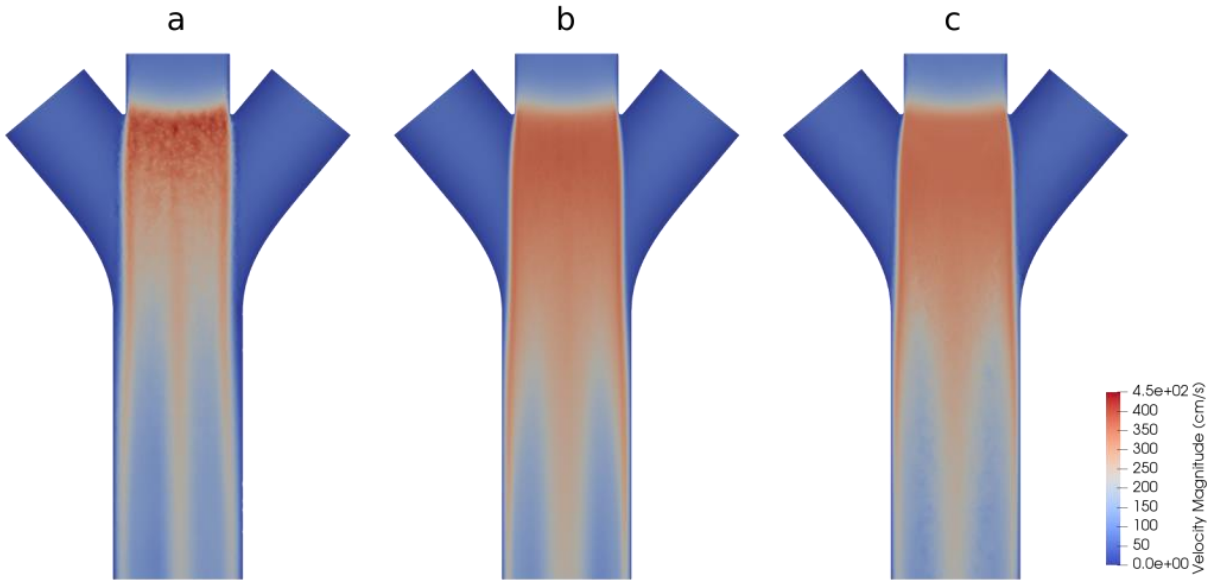

Figure 4. Flow velocity magnitude result comparison for simulations performed with a) coarse uniform mesh with 1 million elements, b) fine uniform mesh with 10 million elements, and c) adaptively refined mesh with 2 million elements.

Aortic pressure regulatory system

The aortic pressure regulatory system is modeled based on the idea of a proportional–integral–derivative (PID) controller.[26] The PID controller calculates a correction term, u(t), from an error value, e(t). The error value is calculated from the difference between the setpoint, SP, and the process variable, PV(t). The formulations are presented in equations 5 and 6, where K_p, K_i, and K_d are the proportional, integral, and derivative gains, respectively.

$$e(t) = SP - PV(t) \quad [5]$$

$$u(t) = K_p e(t) + K_i \int_0^t e(t)dt + K_d \frac{de(t)}{dt} \quad [6]$$

In the pressure regulatory system, the setpoint would be the target mean aortic pressure, which is 67 mmHg. The process variable will be the average aortic pressure obtained from the simulation over the last cardiac cycle. The correction term calculated will be added to the total blood volume to adjust the average aortic pressure.

The first version of the aortic pressure regulatory system only used a proportional controller, K_p, with the frequency of one cardiac cycle. The correction term is calculated after each cardiac cycle using the average aortic pressure of that cycle. This method is extremely easy to implement since the formulation of the total volume, Vol, is very simple as shown in equation 7, where the error is a function of the cardiac cycles, C.

$$Vol_{n+1} = Vol_n + K_p e(C_n) \quad [7]$$

The disadvantages of this method come from the low correction frequency, once per cardiac cycle. The LPN system also has a delayed response to the change in total blood volume due to the capacitors. It takes around 30 cardiac cycles for the average aortic pressure to converge to within 0.1% of the desired value, as shown in figure 5a.

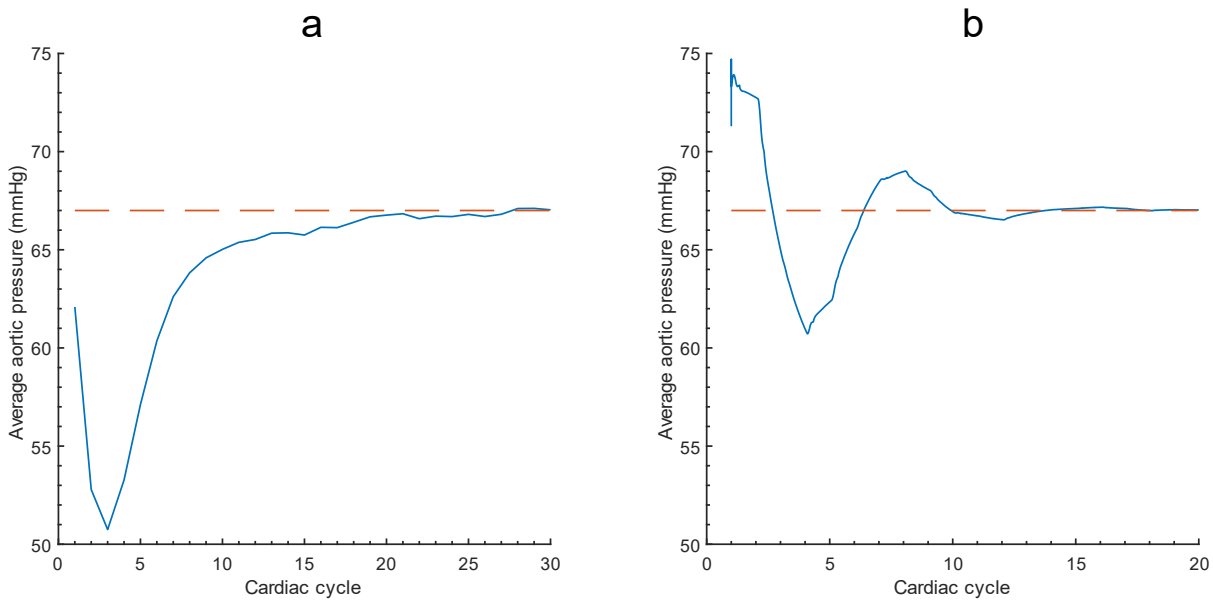

Figure 5. Aortic pressure regulatory system convergence performance for a) proportional controller and b) PID controller.

To achieve faster convergence time and save computational cost, an improved pressure regulatory system was built with the full PID controller. The volume updating equation, therefore, becomes that of equation 8, where the error is a function of the time steps.

$$Vol_{n+1} = Vol_n + K_p e(t) + K_i \int_0^t e(t)dt + K_d \frac{de(t)}{dt} \qquad [8]$$

Formulating the pressure regulatory system this way poses certain challenges. First of all, instead of one average aortic pressure, the LPN needs to track the whole aortic pressure history for the last one cardiac cycle. These additional data could take up a large amount of disk space, but the additional computational cost is considerably less than the computational time for running one cardiac cycle of simulation. Also, the optimal values for the proportional, integral, and derivative gains are difficult and time-consuming. There are various algorithms developed

for tuning a PID controller in literature. Currently, The values of K_p, K_i, and K_d are tuned using the Ziegler–Nichols method [27] to be $2.1 \cdot 10^{-4}$, $2.1 \cdot 10^{-4}$, and $6 \cdot 10^{-5}$, respectively. The convergence is twice faster than the previous method, within 15 cardiac cycles, as shown in figure 5b. However, judging from the overshoot of the convergence plot, the gains are still not optimal. Better tuning methods for the gains could potentially further reduce the convergence time.

Conclusion

Both of the methods, the adaptive mesh and the aortic pressure regulatory system, developed for this study aim for improving the simulation result accuracy and conserving simulation cost. The adaptive mesh refinement significantly reduced the overall error of the simulation with little or no increase in computational cost. The adaptive mesh method also prevents high local errors. The pressure regulatory system, although does not fully represent the complexity of the human autoregulatory system, works efficiently and accurately in controlling the average aortic pressure in our application.

CHAPTER 3

DESIGNING A MODIFIED ASSISTED BIDIRECTIONAL GLENN PROCEDURE TO REALIZE THE EJECTOR PUMP EFFECT

Introduction

In the original design of the ABG, the SVC pressure ought to be lowered by the ejector pump effect, i.e., the shunt flow energy ought to lower the SVC pressure *below* that of the PA. [11] However, all previous studies involving the ABG have consistently failed to demonstrate the ejector pump effect. [11], [14], [15] The objective of this study is to introduce modifications to the original design to successfully realize the ejector pump effect in newborns' circulation and produce an SVC pressure lower than that of the PA. The proposed modifications are assessed and compared against the conventional stage-one operation, mBTS, and the bidirectional Glenn procedure using multiscale CFD simulations[19], incorporated with the simulation methods discussed in chapter 2.

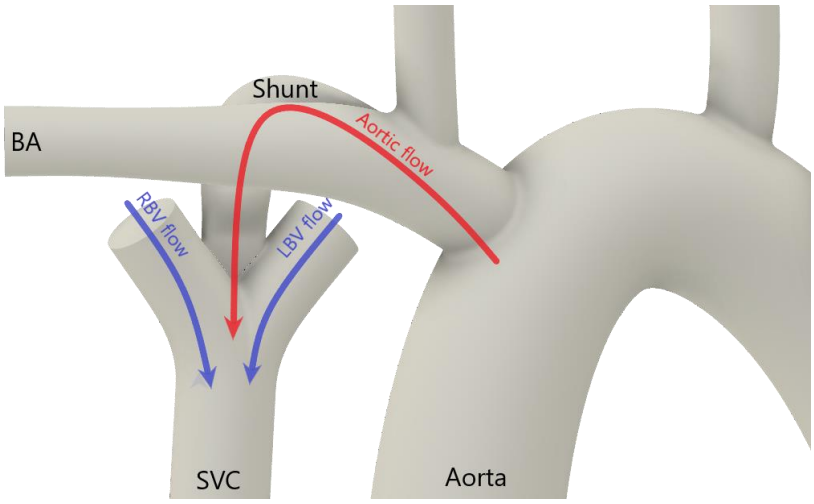

Figure 6. The anastomosis between the shunt and SVC with the nozzle inserted at the venous angle and creates a jet aligned with the SVC flow. BA, brachiocephalic artery (innominate artery); SVC, superior vena cava; RBV, right brachiocephalic vein; LBV, left brachiocephalic vein.

Proposed modifications

The original design of the ABG procedure establishes a shunt between the innominate artery (IA) and the SVC (figures Figure *6* and Figure *7*). High energy fluid from the IA is ejected into the side of the SVC to assist its perfusion into the PA. Ideally, this process will increase the pulmonary flow rate while reducing the upper body (SVC) venous return pressure. This concept, known as the ejector pump effect, is primarily used in industrial applications[11], where ejector pumps typically operate at high velocities (i.e. Reynolds number) to allow for efficient mixing and transfer of energy between two flows. The flow Reynolds number in a single ventricle circulation is much lower than that of an industrial application. Therefore, to allow for the efficient operation of the ejector pump effect in a single ventricle circulation, we propose two modifications. First, the shunt-SVC connection is moved to the venous angle,

between the left and right brachiocephalic veins, to align two flows and utilize a longer mixing region in the SVC. The venous angle may be superior in comparison to the brachiocephalic artery, producing a shunt with a bigger U-shape bend than what we have in our anatomical model. However, we do not anticipate such an adjustment in the simulated geometry changes our results significantly. Second, the shunt cross-sectional geometry at the shunt-SVC connection converges to a slit-shape (Figure Figure *7*). The cross-sections are taken at the nozzle and the downstream is the SVC-PA junction. For clinical implementation, this convergence can be achieved by putting a slit-shaped metal band around the shunt exit to constrain the geometry. This design maximizes the contact area between the high and low velocity flows in the SVC, allowing more effective momentum transfer and thereby improving their mixing.

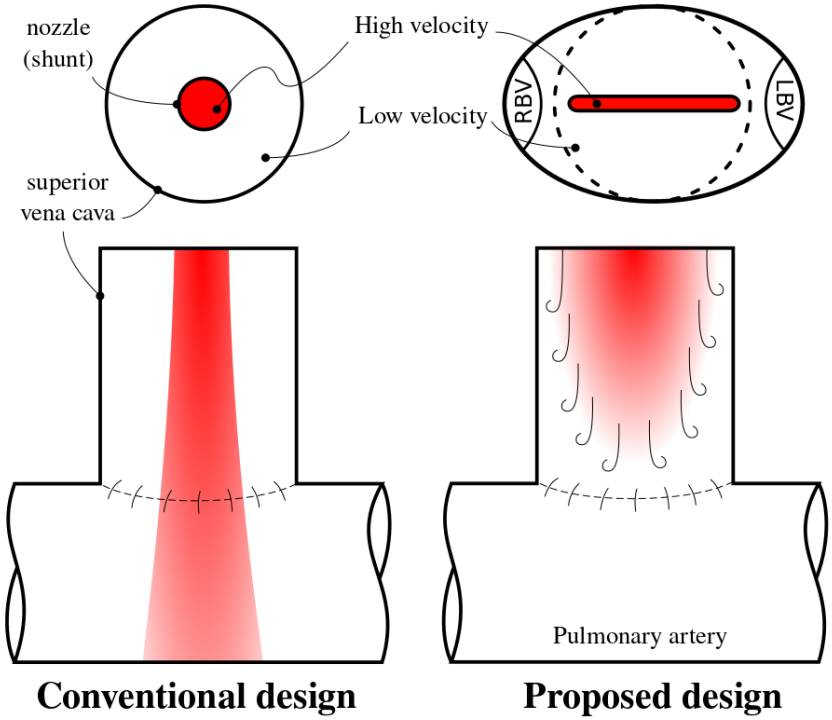

Figure 7. Nozzle inlets diagonal view and SVC-PA connection for the original design (left) and the proposed design (right). The effectiveness of the proposed design in transforming the shunt flow energy to the SVC flow is shown schematically.

Multiscale simulations

To evaluate the effectiveness of the modifications, we employed multiscale CFD simulations that are similar to the previous studies.[11], [14], [15] In these simulations, the flow in major vessels (e.g., aorta, PA, SVC, etc) is fully resolved in 3D while it is modeled for the rest of the circulatory system (e.g., the heart, lower and upper body microvasculature, etc.) using a 0D lumped parameter network (LPN).[19], [28]

Geometry construction

The 3D models of the blood vassals are constructed using Fusion 360 based on similar dimensions of the previous ABG study.[11] Three 3D geometries are constructed in total. The systemic side is unchanged for all three geometries and consists of the aorta, the brachiocephalic trunk, the right common carotid artery, the left common carotid artery, and the left subclavian artery. For the pulmonary side, the pulmonary artery diameter is 5.5 mm for all models. The conventional stage-one anatomy establishes a 3.5 mm modified Blalock Taussig Shunt (mBTS) between the innominate and pulmonary artery. The conventional bidirectional Glenn (BDG) anatomy includes an end-to-side SVC-PA anastomosis where the SVC diameter is 5 mm. The modified ABG (mABG) is modified in comparison to the original ABG anatomy with two changes described in Section 2.1. The SVC diameter is the same as that of the BDG. The left and right brachiocephalic veins diameters are calculated to be 4 mm using Murray's law.[29] The shunt in the mABG is 3.5 mm in diameter which converges to a slit-shaped which is 3.5 mm wide and 0.6 mm thick at the shunt-SVC connection (Figure 7). The selection of the shunt exit shape is discussed in later sections.

Lumped parameter network

The lumped parameter network uses sets of resistors, capacitors, and inductors to model the flow in the body. Based on the previous study[11], the body circulation is divided into five blocks to model the upper body, the lower body, the pulmonary bed, the coronary circulation, and the heart, where the component values are taken from 28 Norwood-procedure patients.[7] To mimic the auto-regulation of blood pressure, the total excess blood volume is adjusted automatically after each simulated cardiac cycle to keep the aortic pressure fixed at 67

mmHg.[7] Pulmonary vascular resistance of 2.3 and 7 Wood units-m^2 are simulated for all three procedures to model patients with normal and elevated PVR.

CFD simulation

For the 3D simulation, incompressible Newtonian fluid and rigid walls are assumed. Blood density is 1060 kg/m^3 and viscosity is 0.004 Pa-s. The computational mesh is discretized using 4.1, 3.4, and 2.8 million tetrahedral elements for mBTS, BDG, and mABG, respectively. Each mesh is highly adapted using a method that calculates the required element size as a function of the second gradient of the flow velocity.[22] This method ensures the accuracy of our simulations despite the presence of a large velocity gradient in the nozzle and SVC. Simulations are performed using a validated in-house finite-element solver.[19]–[21] The time step of the 3D solver is 0.25 ms for mBTS and BDG and 0.1 ms for mABG. A minimally intrusive backflow stabilization method is used to avoid simulation divergence due to backflow on the outlets.[30] In total, six simulations were run for three geometries at normal and elevated PVR.

Results

Numerical results for six simulated cases are presented in Table 1. The simulated quantities for the mBTS are within one standard deviation of the reference clinical measurements.[7] Also, consistent with the previous studies, the mABG, and BDG heart workload is approximately half that of the mBTS at both PVR. In comparison to the mBTS, the pulmonary blood flow rate is approximately halved in BDG, whereas the pulmonary flow is reduced by 20% to 30% in the mABG at normal to high PVR. The mABG procedure also has the highest oxygen delivery and

aortic oxygen saturation among three procedures at both normal and high PVR. Most importantly, the present mABG lowers the SVC pressure below the PA pressure. At normal PVR, the SVC pressure in mABG is lower than that of the BDG despite a significantly higher PA flow rate.

Table 1: Simulation results of Modified Blalock-Taussig shunt (mBTS), bidirectional Glenn (BDG), and modified assisted bidirectional Glenn (mABG) at normal (2.3 Wood unit-m^2) and high PVR (7 Wood unit-m^2). Percentage changes are compared to mBTS.

PVR	**Normal**					**High**				
Model	mBTS	BDG		mABG		mBTS	BDG		mABG	
$OD, mL_{O_2}/s$	2.72	2.97	*+9%*	3.16	*+16%*	2.65	2.74	*+3%*	2.86	*+8%*
OD_{cor}, mL_{O_2}	0.20	0.22	*+10%*	0.21	*+5%*	0.19	0.20	*+5%*	0.20	*+5%*
$HL, Nm/min$	18.9	6.6	*-65%*	9.9	*-48%*	16.7	6.3	*-62%*	8.9	*-47%*
$CO, L/min$	2.08	1.07	*-49%*	1.43	*-31%*	1.93	1.02	*-47%*	1.32	*-32%*
Q_P/Q_S	1.21	0.46	*-62%*	0.88	*-27%*	1.01	0.44	*-56%*	0.82	*-19%*
$Q_S, L/min$	0.94	1.07	*+14%*	1.00	*+6%*	0.96	1.02	*+6%*	0.93	*-3%*
$Q_P, L/min$	1.14	0.50	*-56%*	0.88	*-23%*	0.97	0.45	*-54%*	0.76	*-22%*
$Q_{lb}, L/min$	0.53	0.57	*+8%*	0.56	*+6%*	0.54	0.57	*+6%*	0.56	*+4%*
$Q_{ub}, L/min$	0.41	0.50	*+22%*	0.44	*+7%*	0.42	0.45	*+7%*	0.37	*-12%*
$Q_{cor}, L/min$	0.07	0.08	*+14%*	0.07	*0%*	0.07	0.08	*+14%*	0.07	*0%*
$P_{ao}, mm\ Hg$	67.1	66.9	*-0%*	67.0	*-0%*	67.0	67.1	*+0%*	67.0	*0%*
$P_{SVC}, mm\ Hg$	2.9	5.8	*+100%*	**4.3**	*+48%*	2.6	11.7	*+350%*	14.5	*+458%*
$P_{PA}, mm\ Hg$	11.0	5.0	*-55%*	**8.3**	*-25%*	23.4	11.0	*-53%*	18.1	*-23%*
$PP_{PA}, mm\ Hg$	5.57	3.32	*-40%*	4.83	*-13%*	7.84	2.72	*-65%*	5.45	*-30%*
PI_{PA}	0.84	1.00	*+19%*	0.57	*-32%*	0.9	0.66	*-27%*	0.44	*-51%*
Q_{LPA}/Q_{RPA}	0.85	1.00	*+18%*	1.00	*+18%*	0.94	1.00	*+6%*	1.00	*+6%*
$Sat_{ao}, \%$	77.5	74.4	*-4%*	84.7	*+9%*	73.9	72.0	*-3%*	82.6	*+12%*

OD, systemic oxygen delivery; OD_{cor}, coronary oxygen delivery; HL, workload on the single ventricle; CO, cardiac output; Q_P, pulmonary average flow rate; Q_S, systemic average flow rate; Q_{lb}, lower-body average flow rate; Q_{ub}, upper-body average flow rate; Q_{cor}, coronary average flow rate; P_{ao}, aortic average pressure; P_{SVC}, superior vena cava average pressure; P_{PA},

pulmonary artery average pressure; PP_{PA}, pulmonary artery average pulse pressure; PI_{PA}, pulmonary artery average pulsatility index; Sat_{ao}, aortic percentage oxygen saturation.

Discussion

The high SVC pressure was one of the major concerns in the ABG procedure. Previous studies consistently showed that the ABG produces an SVC pressure that exceeded that of the mBTS and BDG at normal and high PVR to a level that may not be tolerated by infants. The two modifications featured in mABG, reported here, aim to lower the SVC pressure by improving mixing and reducing energy loss. The first modification of moving the shunt insertion location upstream reduces the loss of energy caused by the high-velocity jet going into the SVC wall at an angle in the original ABG. The second modification that changes the nozzle shape requires more consideration. The goal of the irregular shape is to increase the contact area of the two flows and induce instability to trigger turbulent mixing downstream (Figure 8). Better mixing will result in more energy transferred into the upper body return flow and therefore reduce SVC pressure. However, since turbulence dissipates energy, excessive turbulence will be counter-effective. The slit-shape nozzle proposed provides the best balance between sufficient mixing and limited turbulence, as well as low viscous loss inside the converging area of the nozzle. In the end, the proposed mABG lowered the SVC pressure to 4.3 mmHg at normal PVR, a value that potentially avoids upper-body edema and SVC syndrome.[16]

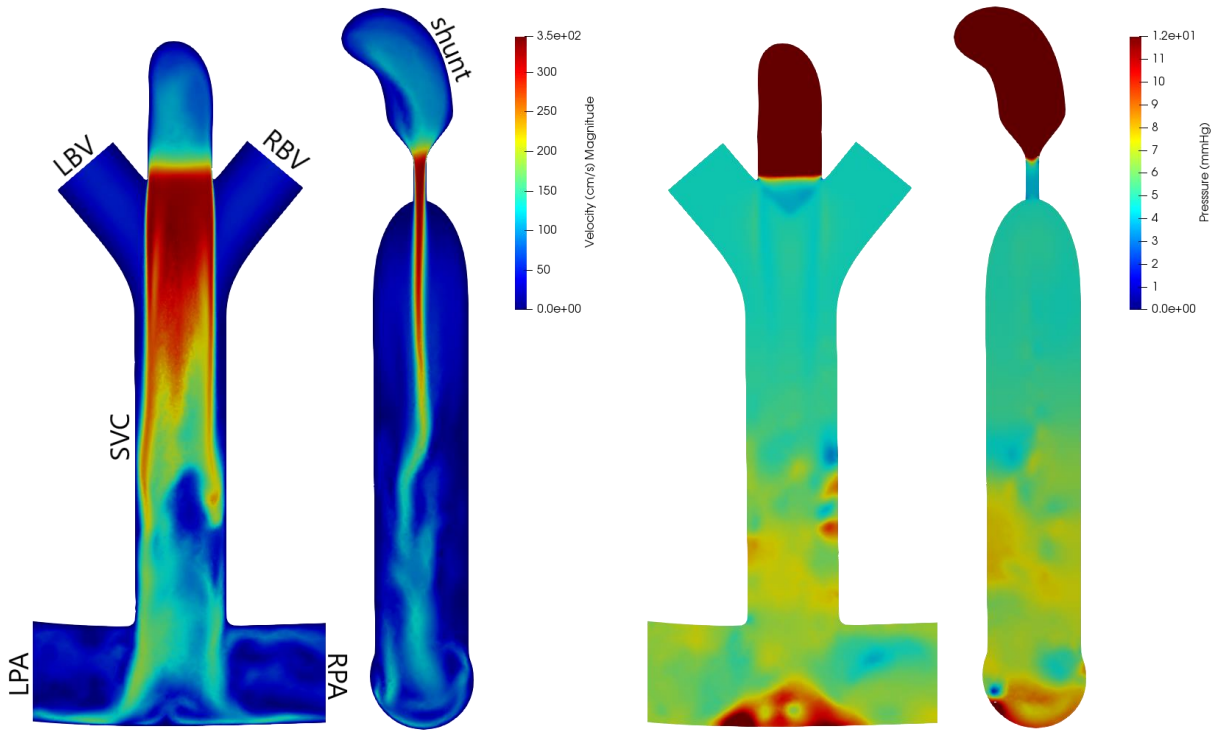

Figure 8. Velocity (left) and pressure (right) contours of the shunt, BVs, SVC, and PAs at normal PVR. Slices on the left are along the nozzle center-line and slices on the right are perpendicular to the nozzle.

The effectiveness of the proposed modifications can be further analyzed by considering the difference between SVC and PA pressures. The SVC pressures in previous studies of the ABG were consistently higher than that of the PA, indicating ineffectiveness in implementing the ejector pump effect.[11], [14], [15] In this study, the ejector pump effect is demonstrated and the SVC pressure is significantly lowered in comparison to its baseline PA pressure. More specifically, the SVC pressure was 1.5 mmHg higher than the PA pressure in the original design of the ABG,[11] whereas it is approximately 4 mmHg lower than the PA pressure in the mABG. These numerical results show that the combination of the lengthened mixing region and improved upstream mixing efficiency leads to an overall ejector pump design that effectively operates at low Reynolds number (~1000) when placed in neonatal anatomy.

Flow pulsatility in the pulmonary arteries is important for PA growth. Studies have shown that patients who received early BDG procedures have higher tendencies to develop PA stenoses because BDG provides less pulsatility than mBTS.[31], [32] The proposed mABG design has lower pulse pressure than the mBTS but higher than that of the BDG procedure. As for the pulsatility index, which is calculated by normalizing the peak-to-peak velocity by the mean velocity, the BDG has the greatest value of pulsatility index primarily due to its lowest mean velocity. Further studies need to determine whether such a reduction in pulsatility impedes PA growth in the mABG at earlier stages of infancy. Another disadvantage of mBTS is the uneven flow distribution between LPA and RPA resulting in uneven PA growth.[33] The mABG procedure provides even flow distribution between the LPA and RPA.

In contrast to these encouraging outcomes at normal PVR, the SVC pressure remains relatively high at elevated PVR. The PA pressure scales with the PVR while the ejector pump pressure recovery does not, resulting in an SVC pressure three times higher than that of a normal PVR. In practice, the PVR of newborns is elevated up to 3-6 weeks, during which a high SVC pressure could have devastating effects.

Despite the high SVC pressure at elevated PVR, the ABG with some changes may still be considered as a surgical option for infants experiencing episodes of elevated PVR. Historically, the BDG was not performed as the stage-one operation due to complications related to high PVR. According to early clinical data, SVC syndrome was the major cause of death for patients with high PVR,[10], [34] with only one out of eight deaths caused by cerebral damage.[10]

More recent studies have shown the feasibility of performing the BDG operation at earlier ages.[8], [9] Lower oxygen saturation after surgery, which results in longer ICU stay, was the major concern for not performing the operation before two months of age. This observation agrees with our simulation showing the oxygen saturation is the lowest for the BDG. Our simulation shows that the mABG provides 69% greater pulmonary perfusion and 13% greater oxygen saturation compared to the BDG at elevated PVR, which cumulatively could reduce the risk of SVC syndrome and address the concern for low oxygen saturation. Additionally, clinical measurements showed that the average SVC pressure in patients undergoing an early BDG operation is as high as 13.2 mmHg.[8] The low rate of mortality and morbidity in this group of patients indicates that even the high SVC pressure produced by the mABG at elevated PVR may well be tolerated by the patients. If needed, a lower SVC pressure in the mABG can be achieved by either optimizing the geometry or reducing the size of the nozzle as it will lower the aortic-to-pulmonary flow and thus PA and SVC pressures. Therefore, a more comprehensive study is needed before one can extend the reasoning provided for the failure of the BDG procedure in newborns with high PVR to the mABG procedure.

The 90° angle at the SVC-PA anastomosis is not ideal for a smooth flow transition. The pressure results in Figure 3 show a significant pressure stagnation region at the bottom of the PA due to flow impingement. To understand the impact of the stagnation on flow rate and pressure recovery, a Y-shaped SVC-PA junction was simulated (not shown here). The design of the junction is inspired by the several Y-graft proposals [35]–[37] in Fontan patients to improve hepatic flow distribution as well as lower inferior vena cava pressure. The Y-junction resulted in a smoother transition of flow and a smaller stagnation region. The pulmonary flow

rate was increased by 5% and the SVC pressure was reduced further by 20%. However, clinically adapting the Y-graft is extremely difficult and more complex than necessary.[38] Therefore, the detailed results of the Y-shaped junction design are not included in Table 2. Future studies should nonetheless consider the possibility of improving the SVC-PA flow transition to the extent that the clinical practice allows.

High shear stress induced by the jet flow causes blood cell trauma. The highest shear stress in the mABG occurs near the diverging nozzle wall and is 4200 $\mathrm{dynes/cm^2}$, with an exposure time of approximately 10^{-4} second. In the rest of the mABG anatomy, the shear stress remains below 1000 $\mathrm{dynes/cm^2}$. These shear stress levels will unlikely cause red blood cell damage but will likely trigger platelet activation.[39], [40] Thromboses formation in the nozzle and SVC is a potential hazard to be studied in detail in the future. The shunt occlusion in the mABG is less risky than that of the mBTS as it is merely a transition to the BDG circulation. Theoretically, the shunt should remain patent until patients can tolerate the BDG circulation which, based on the timing of the stage-two operation, is about four months.[3] Future studies should incorporate multi-constituent simulations[41] to assess the risk of thrombosis and provide a guideline for further customization of the ABG for neonates.

Limitations

One of the limitations of our computational framework is the assumption of rigid walls. However, previous Fontan and mBTS simulations have demonstrated that this assumption has limited effects on pressure and flow.[11], [42] Another limitation includes the assumption of

Newtonian fluid for blood, although strain rates are not within a range to produce non-Newtonian effects. The venous angle geometry was built according to Murray's law and not clinical data. Thrombus formation is not modeled during this study. More vigorous studies on shunt occlusion need to be performed before any clinical consideration. Surgical difficulties, such as precision of shunt alignment or shunt stabilization, are not considered for this study. The nozzle design is specific to the SVC and PAs dimensions chosen in this study; however, preliminary results show it can be successfully scaled to patient-specific geometries, warranting more realistic multiscale modeling of these circulations in the future.

Conclusion

This study demonstrated a modified ABG design that was able to preserve all advantages of the original ABG procedure while reducing the SVC pressure at normal PVR. This study marks the first successful adaptation of the ejector pump effect in the ABG circulation. Although there is no significant improvement in the SVC pressure for high PVR, the modeling and simulation methods developed in this study can be used for future studies. Future optimization and parametric study will aim to improve and characterize the ABG hemodynamics efficiency for a broader range of conditions.

CHAPTER 4

OPTIMIZATION OF THE PROPOSED MODIFIED ASSISTED BIDIRECTIONAL GLENN PROCEDURE

Introduction

In the previous chapter, we demonstrated the successful adaption of the ejector pump design for infants with single-ventricle physiology. The shunt insertion location aligned the high-velocity flow with the SVC flow and the slit-shaped nozzle improved mixing between the high-velocity jet and the upper body return flow. The modifications resulted in 4 mmHg of pressure recovery at the PA compared to the SVC inlet, while successfully reducing the SVC pressure to 4.3 mmHg at normal PVR. These encouraging results make the ABG procedure more plausible towards surgical implementation. Further optimization is nonetheless required to fully realize the pressure reduction potential of the proposed modification at normal PVR. Despite the results at normal PVR, one problem remains unsolved in the previous chapter as well as the original ABG study[11]. At high PVR, the SVC pressure is considerably high for the original ABG configuration, predicted to be 14.9 mmHg. Our modified ABG, although demonstrating a pressure recovery of 2.6 mmHg, caused an increase in the SVC pressure to 14.5 mmHg at high PVR. These considerations motivated an optimization study focusing on the shunt exit nozzle geometry.

For the optimization study, the design objective is to minimize the SVC pressure for a given PVR value. The SVC pressure is affected by 1) the total energy injected into the pulmonary side and 2) the total energy loss in the ejector pump. Since the pressure upstream at the aorta is

controlled at 67 mmHg, the area of the nozzle decides the total amount of energy provided to the pulmonary side by controlling the flow rate. As the nozzle increases in size the flow rate to the pulmonary side, the single ventricle workload will also increase. For the optimization of the nozzle area, the resulting heart load also needs to be kept in a reasonable range. Therefore, we built a theoretical model for the pressure recovery in the SVC, which is calculated from the fixed parameters of the study with several simplified assumptions. The modeling of the theoretical calculation is discussed in the following section. From this theoretical value, the ejector pump efficiency can then be calculated by taking the ratio to the actual pressure recovery from the simulation. Lower ejector pump efficiency will suggest relatively more energy loss in the system and less efficient design.

To improve the efficiency of the design and achieve lower SVC pressure, other parameters related to energy loss are considered. For this study, three major parameters are considered: the width of the nozzle opening, the length of the nozzle, and the diameter of the shunt. Some of the simulations were performed before the nozzle is changed to a non-intrusive nozzle and some of the simulations were performed on the Y-shaped SVC-PA connection. The differences are demonstrated in figure 9. All the other dimensions and shapes remained the same as the model in chapter one. For each parameter, the base geometries are controlled the same. Due to computational cost consideration, the optimization simulations were not repeated based on the final geometry in chapter one. We assume that the parametrical optimums regarding the nozzle design are independent of the intrusiveness of the nozzle and the downstream connection. However, this assumption does not necessarily hold. For future optimization study, the base geometry should be fixed among all parameters for a more accurate optimal design.

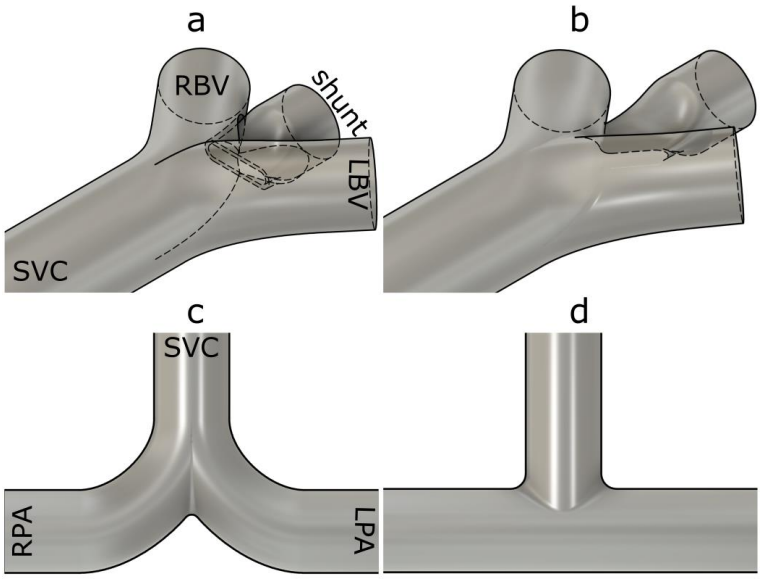

Figure 9. Geometries of a) intrusive systemic-pulmonary shunt nozzle, b) non-intrusive systemic-pulmonary shunt nozzle, c) Y-shaped SVC-PA junction, and d) T-shaped SVC-PA junction.

For the nozzle area study, the base model has an intrusive nozzle and a Y-shaped SVC-PA connection. The nozzle area is adjusted only by changing the nozzle thickness, t, which is considered to have the smallest effect on the hydrodynamics of the system. For the nozzle width study, the base model was an intrusive nozzle but with a conventional T-shaped SVC-PA connection. The nozzle length study has the same base geometry as the nozzle area study with nozzle area of 2.245 mm^2. Lastly, the shunt diameter study is modified from the final design of chapter one, modifying both shunt diameter and nozzle width to 4 mm. The rationale behind this modification will be discussed in the later sections.

Theoretical calculation

To quantify the overall efficiency of the nozzle design, we used a 0-dimensional mathematical model to calculate the theoretical pressure recovery without energy loss (figure 10). The fluid is assumed incompressible， inviscid, and one-directional. The calculation schematics are shown in figure 10. The cross-sectional areas are measured from the modified ABG model. The pressure at nozzle upstream, P_{H1}, is considered a fixed known value of 67 mmHg since the aortic pressure is automatically regulated. The total flow rate from the upper body, Q_{ub}, is also considered a fixed value at 0.43 L/min since the systemic flow is not influenced by the change in shunt or nozzle design. Since the flow is assumed incompressible, the velocities at upper body return, V_L, can be calculated by conservation of mass.

$$V_L = \frac{Q_{ub}}{A_{SVC}} \qquad [9]$$

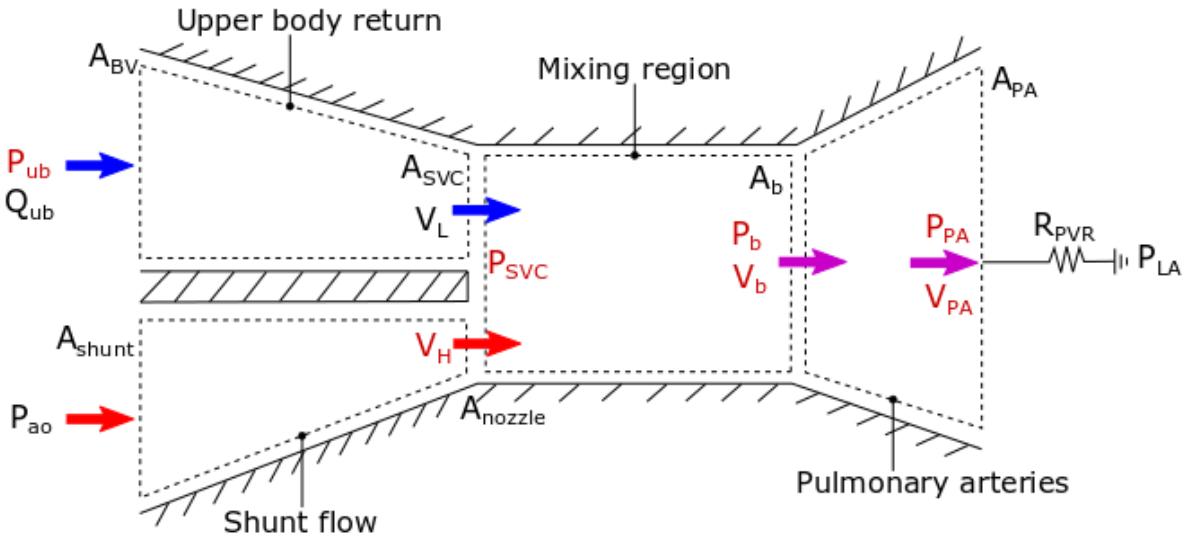

Figure 10. Theoretical calculation model schematics. Unknown values are marked in red.

For normal PVR, the downstream resistance, R_{PVR}, is 2.3 Wood units-m^2. Three Bernoulli's equations can be written for the shunt flow, upper body return, and pulmonary arteries control volumes, as in equations [10, [11, and [12] respectively. Note that the P_{ub} value, not the P_{SVC} value, corresponds to the SVC pressure reported in the simulation.

$$P_{ao} = P_{SVC} + \frac{1}{2}\rho V_H^2 \quad [10]$$

$$P_{ub} + \frac{1}{2}\rho V_{ub}^2 = P_{SVC} + \frac{1}{2}\rho V_L^2 \quad [11]$$

$$P_b + \frac{1}{2}\rho V_b^2 = P_{PA} + \frac{1}{2}\rho V_{PA}^2 \quad [12]$$

For the mixing region, two equations are written: conservation of mass (equation [*13*) and conservation of momentum (equation [14).

$$V_L A_{SVC} + V_H A_{nozzle} = V_b A_b \quad [13]$$

$$\rho V_L^2 A_L + \rho V_H^2 A_H + P_{SVC}(A_L + A_H) = \rho V_b^2 A_b + P_b A_b \quad [14]$$

Two additional equations are the conservation of mass in the pulmonary artery section (equation [15) and the pressure flow relationship at the flow exit (equation [16).

$$V_b A_b = V_{PA} A_{PA} \quad [15]$$

$$\frac{P_{PA}}{V_{PA}/A_{PA}} = R_{PVR} \quad [16]$$

In total, there are five equations and five unknowns: P_{ub}, P_{SVC}, P_b, P_{PA}, V_H, V_b, and V_{PA}. Because equation [14 is a second-order equation, it will give two sets of solutions. Only one of the solutions will have the fluid flowing in the correct direction from the inlets to the outlet, which is considered the actual physical solution. The only changing variable for this

theoretical calculation is the nozzle area, A_{nozzle}. Therefore, the theoretical trends of the upper body pressure, pulmonary artery pressure, and pressure recovery as the nozzle area changes can be plotted, as shown in figure 11. The x-axis is a non-dimensional nozzle area calculated by dividing the nozzle area by the total SVC cross-sectional area.

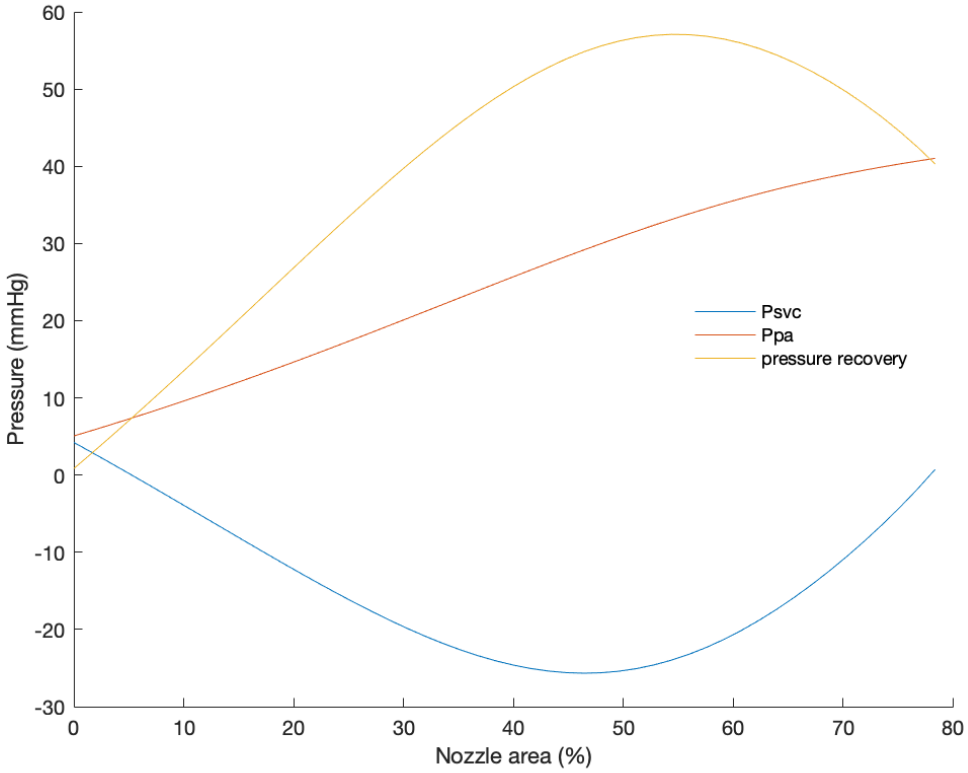

Figure 11. Theoretical values of the SVC pressure, PA pressure, and pressure recovery as functions of the shunt nozzle area.

The calculated theoretical upper body pressure represents the lowest possible SVC pressure for the given nozzle area. However, whether the trends hold in the simulation still depends on the efficiency of the ejector pump. The ejector pump efficiency, EP_{eff}, is calculated as the ratio of

theoretical pressure recovery, ∇P_{th}, and simulated pressure recovery, ∇P_{CFD}, where pressure recovery is the difference between pulmonary artery pressure and the SVC pressure, as shown in equations [17 and [18.

$$EP_{eff} = \nabla P_{CFD} / \nabla P_{th} \quad [17]$$

$$\nabla P = P_{PA} - P_{SVC} \quad [18]$$

Multiscale simulation

The optimization study used the same modeling software, Fusion 360, as the previous study. The adaptive mesh method also remains unchanged. As for the simulation, the same in-house 3D fluid solver was used. [19]–[21] The schematics and the component values of the lumped parameter network are also the same.[7] Both variations of the regulatory system were used for different simulations. This difference only affects the computational cost but not the result accuracy. All adaptive meshes used six iterations and an error tolerance of 0.2. The simulations were run with a time step size of 10^{-4} seconds.

Results

The optimization results are presented in this section. Parameters considered are nozzle area, A, nozzle width, W, nozzle length, L, and shunt diameter, D_{shunt}, as marked in figure 12.

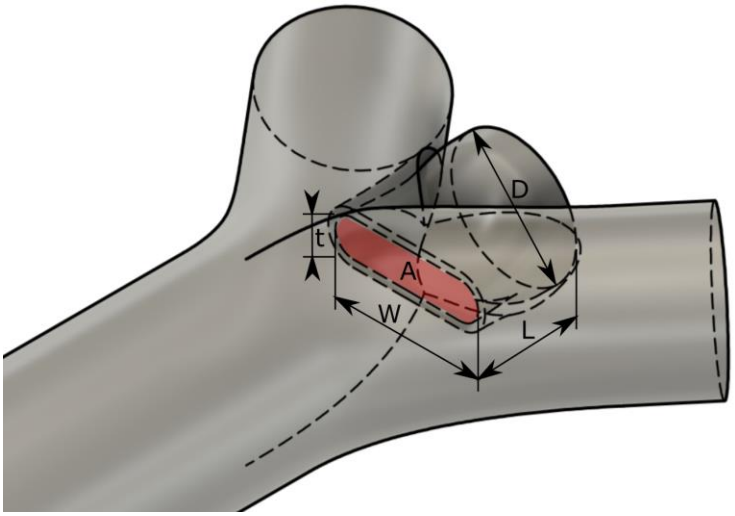

Figure 12. Nozzle optimization parameters. A, nozzle area; W, nozzle width; L, nozzle length; D, shunt diameter; t, nozzle thickness.

Nozzle area, A

The base model of the area study has an intrusive nozzle and a Y-shaped SVC-PA connection. The nozzle width, nozzle length, and shunt diameter are fixed at 4 mm, 2.5 mm, and 3.5 mm, respectively. The change in the nozzle area is achieved by changing the nozzle thickness, t. Nozzle areas of 2.25, 2.75, 3.30, and 3.78 mm^2 are simulated. The results are summarized in Table 2.

Table 2. Simulation result of modified assisted bidirectional Glenn models with different systemic-pulmonary shunt nozzle areas.

PVR	Normal			
Area, mm^2	2.25	2.75	3.30	3.78
$OD, mL_{O_2}/s$	3.14	3.25	3.32	3.26
$OD_{cor}, mL_{O_2}/s$	0.29	0.21	0.20	0.34
$HL, Nm/min$	10.1	11.1	11.9	12.9

$CO, L/min$	1.44	1.54	1.61	1.70
Q_P/Q_S	0.90	0.98	1.08	1.16
$Q_S, L/min$	0.99	1.00	0.99	0.99
$Q_P, L/min$	0.89	0.99	1.08	1.15
$Q_{lb}, L/min$	0.56	0.56	0.55	0.55
$Q_{ub}, L/min$	0.43	0.45	0.44	0.44
$Q_{cor}, L/min$	0.09	0.06	0.06	0.10
$P_{ao}, mm\ Hg$	67.0	67.2	66.8	67.1
$P_{SVC}, mm\ Hg$	5.3	3.4	3.3	3.7
$P_{PA}, mm\ Hg$	8.4	9.3	10.1	10.7
$Sat_{ao}, \%$	84.8	86.2	87.1	87.8
$EP_{eff}, \%$	25.5	39.8	38.3	34.5

Four values that are not affected by the change in nozzle areas are the systemic flow rate, upper and lower body flow rate, and average aortic pressure. This is anticipated since the systemic geometry is not changed and the average aortic pressure is controlled to be 67 mmHg.

Six values change linearly with the change of area: the single ventricle workload, the cardiac output, the pulmonary to systemic flow ratio, the pulmonary flow rate, the pulmonary artery pressure, and the aortic oxygen saturation. The linear regression and r-squared values are summarized in Table 3.

Table 3. Linear regression and r-squared values of the values (y) that change linearly with the nozzle area (x).

Variable (y)	Linear Regression Equation, Area (x)	R-squared value
$HL, Nm/min$	y = 1.7818x + 6.121	0.9956
$CO, L/min$	y = 0.1646x + 1.0756	0.9932
Q_P/Q_S	y = 0.1708x + 0.5145	0.9993
$Q_P, L/min$	y = 0.1689x + 0.5178	0.9955

P_{PA}, mm Hg	y = 1.4946x + 5.1131	0.9941
Sat_{ao}, %	y = 1.9213x + 80.675	0.9762

Five values fit better under second-order polynomial trends: the systemic oxygen delivery, the coronary oxygen delivery, the coronary average flow rate, the SVC average pressure, and the ejector pump efficiency. The curve fit equations, the r-squared values, and the projected maxima or minima location (nozzle area) are summarized in Table 4. The regression is valid between areas of 2.25 and 3.78 mm^2. The regression curve for the SVC pressure is presented in figure 13a.

Table 4. Summary of polynomial regression, r-squared values, and maxima or minima locations.

Variable (y)	Polynomial Regression Equation, Area (x)	R-squared value	Maxima/Minima area (cm^2)
$OD, mL_{O_2}/s$	$y = -0.1629x^2 + 1.0656x + 1.5643$	0.9775	3.27
$OD_{cor}, mL_{O_2}/s$	$y = 0.2142x^2 - 1.2646x + 2.0539$	0.9685	2.95
$Q_{cor}, L/min$	$y = 0.0682x^2 - 0.4055x + 0.6571$	0.9929	2.97
P_{SVC}, mm Hg	$y = 2.2276x^2 - 143.72x + 26.27$	0.9667	3.23
EP_{eff}, %	$y = -0.1771x^2 + 1.1165x - 1.3522$	0.9291	3.15

Since there are only four data points for each value, the polynomial regression curves are not fitted as well as previous values that are linearly fitted, as indicated by the lower r-squared values. More nozzle areas need to be simulated to find the real relationship between the nozzle area and the variables, which could not necessarily be polynomial regressions. Moreover, the projected maxima or minima locations are all between the data points of 2.75 mm^2 and 3.30 mm^2 nozzle area. More simulations need to be run between these two areas for better confidence in finding the true optimal location.

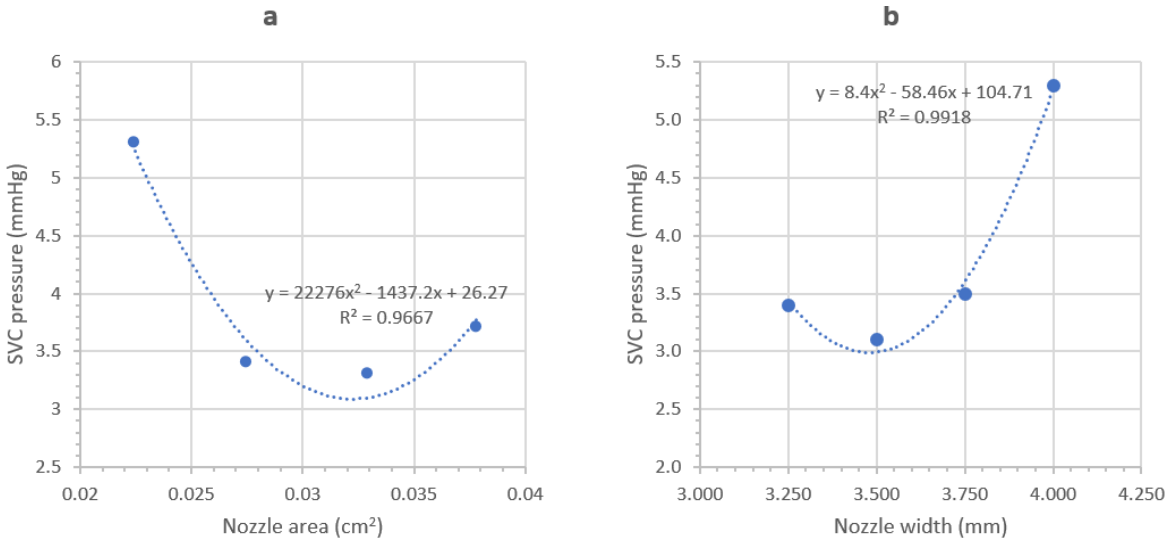

Figure 13. Polynomial regression for a) SVC pressure as a function of nozzle area and b) SVC pressure as a function of nozzle width.

Nozzle width, W

The nozzle width study uses the intrusive nozzle and Y-shaped SVC-PA connection as the base model, the same as the area study. The nozzle area, nozzle length, and shunt diameter are fixed at 2.25 nm^2, 2.5 mm, and 3.5 mm, respectively. Nozzle widths of 4, 3.75, 3.5, 3.25, and 3 mm are simulated. The results are summarized in Table 5.

Table 5. Simulation result of modified assisted bidirectional Glenn models with different systemic-pulmonary shunt nozzle widths.

PVR	Normal			
Width, mm	4.00	3.75	3.50	3.25
$OD, mL_{O_2}/s$	3.14	3.22	3.22	3.23
$OD_{cor}, mL_{O_2}/s$	0.29	0.22	0.21	0.21

$HL, Nm/min$	10.1	10.0	10.1	10.2
$CO, L/min$	1.44	1.45	1.45	1.45
Q_P/Q_S	0.90	0.88	0.88	0.90
$Q_S, L/min$	0.99	1.01	1.01	1.01
$Q_P, L/min$	0.89	0.90	0.89	0.91
$Q_{lb}, L/min$	0.56	0.56	0.56	0.56
$Q_{ub}, L/min$	0.43	0.45	0.46	0.45
$Q_{cor}, L/min$	0.09	0.07	0.07	0.07
$P_{ao}, mm\ Hg$	67.0	67.3	67.0	67.0
$P_{SVC}, mm\ Hg$	5.3	3.5	3.1	3.4
$P_{PA}, mm\ Hg$	8.4	8.5	8.5	8.6
$Sat_{ao}, \%$	84.8	84.9	84.9	85.1
$EP_{eff}, \%$	25.5	41.1	44.4	42.8

The change in nozzle width does not have a significant impact on the hemodynamics for the last three models. However, for the model with a 4 mm wide nozzle, the circulation is different from the others. The differences are likely to be caused by higher impedance inside the SVC. Two results can nonetheless be well fitted to a second-order polynomial: the SVC average pressure and the ejector pump efficiency. The results are presented in Table 6. The regression is valid between widths of 3.25 and 4 mm and the curve is presented in figure 13b.

Table 6. Summary of polynomial regression, r-squared values, and the maxima or minima widths.

Variable (y)	Polynomial Regression Equation, Width (x)	R-squared value	Maxima/Minima width (mm)
$P_{SVC}, mm\ Hg$	$y = 8.4x^2 – 58.5x + 104.7$	0.9918	3.48
$EP_{eff}, \%$	$y = -6906.2x^2 + 4786.6x - 783.81$	0.9880	3.47

Both polynomial regressions have excellent fit to data ($R^2 \approx 0.99$). The maxima are both located very close to a nozzle width of 3.5 mm. Based on further hydrodynamics analysis from the simulation, which will be discussed in the discussion section, we argue that the optimum nozzle width is the same value as the systemic-pulmonary shunt diameter.

Nozzle length, L

The nozzle length study uses the same base model as the previous two studies: intrusive nozzle and Y-shaped SVC-PA connection. The nozzle area, nozzle width, and shunt diameter are fixed at 2.25 mm^2, 3.5 mm, and 3.5 mm, respectively. The nozzle lengths modeled are 1, 2, 2.5, 3, and 4 mm. The simulation result is summarized in Table 7.

Table 7. Simulation result of modified assisted bidirectional Glenn models with different systemic-pulmonary shunt nozzle lengths.

PVR	Normal				
Length, mm	1.0	2.0	2.5	3.0	4.0
$\mathrm{OD, mL_{O_2}/s}$	3.22	3.19	3.22	3.19	3.24
$\mathrm{OD_{cor}, mL_{O_2}/s}$	0.22	0.22	0.21	0.21	0.21
$\mathrm{HL, Nm/min}$	10.1	10.1	10.1	10.0	10.1
$\mathrm{CO, L/min}$	1.44	1.44	1.45	1.44	1.46
$\mathrm{Q_P/Q_S}$	0.87	0.89	0.88	0.89	0.88
$\mathrm{Q_S, L/min}$	1.02	1.01	1.01	1.00	1.02
$\mathrm{Q_P, L/min}$	0.88	0.89	0.89	0.89	0.89
$\mathrm{Q_{lb}, L/min}$	0.56	0.56	0.56	0.56	0.56
$\mathrm{Q_{ub}, L/min}$	0.45	0.45	0.46	0.45	0.46
$\mathrm{Q_{cor}, L/min}$	0.07	0.07	0.07	0.07	0.07
$\mathrm{P_{ao}, mm\ Hg}$	67.3	67.2	67.0	67.0	67.3
$\mathrm{P_{SVC}, mm\ Hg}$	3.2	3.0	3.1	2.9	3.1
$\mathrm{P_{PA}, mm\ Hg}$	8.4	8.5	8.5	8.5	8.5

$Sat_{ao}, \%$	84.8	84.9	84.9	84.9	84.9
$EP_{eff}, \%$	42.3	44.7	44.4	45.5	44.5

There is no significant change or trend in the values reported as the nozzle length changes. Therefore, no regression or optimum is reported. The choice of the nozzle length is therefore up to other considerations such as the likelihood of recirculation inside the nozzle, which may lead to thrombus formation.

Shunt diameter, D

The shunt diameter study is modeled according to the insight gained from the nozzle width study, assuming the optimal nozzle width equals to the shunt diameter. The model is modified from the final model of chapter one with a non-intrusive nozzle and a T-shaped SVC-PA junction, with shunt diameter and nozzle width both changed to 4 mm. The nozzle thickness is adjusted correspondingly to keep the nozzle area the same at 2.25 mm^2. The result is summarized in Table 8 with a comparison to the chapter one result for shunt diameter 3.5 mm.

Table 8. Simulation result of modified assisted bidirectional Glenn models with different systemic-pulmonary shunt diameters.

PVR	Normal	
Diameter, mm	3.5	4.0
$OD, mL_{O_2}/s$	3.16	3.14
$OD_{cor}, mL_{O_2}/s$	0.21	0.21
$HL, Nm/min$	9.9	10.1
$CO, L/min$	1.43	1.43
Q_P/Q_S	0.88	0.89
$Q_S, L/min$	1.00	0.99

Q_P, L/min	0.88	0.88
Q_{lb}, L/min	0.56	0.56
Q_{ub}, L/min	0.44	0.43
Q_{cor}, L/min	0.07	0.07
P_{ao}, mm Hg	67.0	67.4
P_{SVC}, mm Hg	4.3	5.1
P_{PA}, mm Hg	8.3	8.3
Sat_{ao}, %	84.7	84.7
EP_{eff}, %	32.9	26.3

Since there are only two data sets, no trend can be determined. However, the only value that shows significant change is the SVC average pressure and the ejector pump efficiency. The original design of a 3.5 mm shunt performs more desirably for both values.

Discussion

For the nozzle area optimization study, the values that change linearly with the area are associated with the increase in flow through the shunt as the nozzle area increases. The cardiac output and the pulmonary flow rate increase with the flow through the shunt. The single ventricle workload changes with increased cardiac output. Since the PVR is constant, the pulmonary artery average pressure increases linearly with the pulmonary flow rate. Because the systemic flow rate remains the same, both the pulmonary-to-systemic flow ratio and the aortic saturation increase linearly as the pulmonary flow rate increases. Although the increase in ventricle workload is not desirable, the increase in workload in our simulated area range is not significant and still much lower than the ventricle workload of the simulated mBTS physiology in chapter one. For the values with polynomial trends, the oxygen delivery and SVC pressure

profile both agreed that the optimum area lies around 3.2 mm^2, or 16% of the SVC cross-sectional area, although the r-squared value is not as convincing as r-squared values for the linear trends. The trend in coronary flow rate and oxygen delivery needs to be further investigated since there is no obvious explanation of why the coronary flow shows a polynomial profile while the heart load increases linearly.

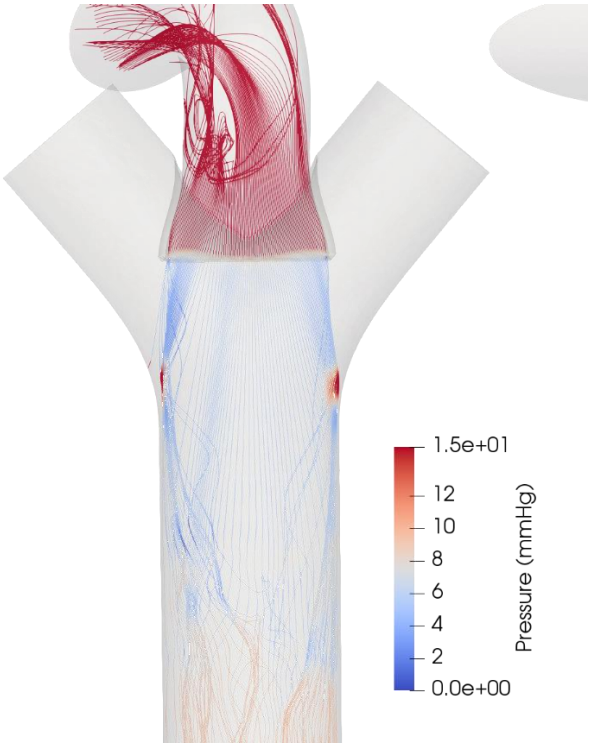

Figure 14. Nozzle flow streamline colored with pressure values for a nozzle width of 4 mm. Two stagnation regions in deep red.

The width study shows drastic differences in the ejector pump effect between the nozzle width of 4 mm and the other three widths. The differences are majorly caused by flow impedance inside the SVC. For the 4 mm wide nozzle, the flow inside the nozzle expands in the width direction, from 3.5 to 4 mm, which results in an expanding high-velocity jet from the nozzle.

The expanding jet will then hit the upper region of the SVC wall, creating two stagnation regions on each side of the SVC wall, as shown in figure 14. Extending this reasoning, any nozzle width that is larger than the shunt diameter will result in an expanding jet from the nozzle, which will likely cause energy loss from impingement on the wall and increase upstream pressure. For nozzle width that is smaller than the shunt diameter, the high-velocity jet will converge. This results in less contact area between the nozzle jet and the upper body return flow and therefore provides less effective mixing. Based on these reasons, the optimal nozzle width should be the same as the nozzle diameter. The regression equation also predicted the optimal nozzle width to be 3.5 mm, which is the same as the nozzle diameter.

The nozzle length study shows no significant differences among the range of length simulated. The choice of the nozzle length, therefore, should be decided by other non-performance related factors. For example, red blood cell survival and platelet activation depend on the level of shear and the exposure time. A shorter nozzle length could be beneficial by shortening the exposure time for blood cells inside the nozzle under high shear. However, the rapid change in geometry for shorter nozzles may create recirculation, which is undesirable for the risk of thrombus formation. The manufacturing or clinical difficulty could be another consideration for nozzle length, as well as growth considerations.

The shunt diameter study took insight from the nozzle width study. The nozzle width is kept the same as the shunt diameter. The result shows that the 4 mm shunt performs worse than the 3.5 mm shunt. Although trends cannot be determined from two simulations, two reasons should be considered to find the optimal shunt diameter. For the mBTS circulation, studies have shown

that shunt occlusion occurs form shunt diameters smaller than 3.5 mm.[43], [44] The mABG circulation is likely to have the same characteristic since the shunt construction is similar. Therefore, if the trend between the values of 3.5 mm and 4 mm shunt is monotonic, due to the constraint to avoid potential shunt occlusion, the optimal shunt diameter would be 3.5 mm. More simulations are required to confirm this assumption.

The Y-shaped SVC-PA connection was proposed during the study in chapter one to reduce the size of the stagnation region at the junction and has demonstrated further SVC pressure reduction by 1 mmHg. The clinical construction of the Y-shaped junction would be extremely difficult if not impossible after consultation with Dr. Tigran Khalapyan. The optimization was performed before the decision to move back to the T-junction. However, since the nozzle optimization most closely relates to the hydrodynamics of the upstream of the SVC, the optimal nozzle design for the T-shaped junction is likely to be very close to that of the Y-shaped junction. The decision to adopt a non-intrusive nozzle was based on input from surgeons on potential complications. The non-intrusive design also improves the ejector pump effect performance by eliminating the flow impedance by the nozzle inside the venous angle. The results observed from the nozzle width and length study is most likely to hold for the non-intrusive nozzle.

For future optimization study, the base geometry of each parameter should be taken from the optimal geometry of the previous parameter. Insights from this study should be used to model the initial geometry since the optimal design for the non-intrusive nozzle and T-shape SVC-PA junction should not be far from the result of this study.

Conclusion

This study performed optimization on the nozzle and shunt geometry of the modified assisted bidirectional Glenn procedure. For the models with intrusive nozzle and Y-shaped SVC-PA junction, the optimal nozzle area is between 2.75 mm^2 (14%) and 3.30 mm^2 (17%), the nozzle width is optimal when it is the same as the shunt diameter, and the nozzle length does not influence the performance significantly. For the models with non-intrusive nozzle and T-shaped SVC-PA junction, a 3.5 mm shunt outperforms a 4 mm shunt. This study provides valuable insights and a starting point for further systematic optimization studies.

REFERENCES

[1] D. C. Fyler, L. P. Buckley, and W. E. Hellenbrand, “Report of the New England Regional Infant Cardiac Program,” *Pediatrics*, 1980, doi: 10.2307/3424295.

[2] P. Khairy, N. Poirier, and L. A. Mercier, “Univentricular heart,” *Circulation*. 2007, doi: 10.1161/CIRCULATIONAHA.105.592378.

[3] Y. d’Udekem *et al.*, “Predictors of survival after single-ventricle palliation: the impact of right ventricular dominance,” *J. Am. Coll. Cardiol.*, vol. 59, no. 13, pp. 1178–1185, 2012.

[4] U. Bartram, J. Grünenfelder, and M. D. Richard Van Praagh, “Causes of death after the modified Norwood procedure: a study of 122 postmortem cases,” *Ann. Thorac. Surg.*, vol. 64, no. 6, pp. 1795–1802, 1997.

[5] M. E. Moghadam, F. Migliavacca, I. E. Vignon-Clementel, T.-Y. Hsia, and A. L. Marsden, “Optimization of shunt placement for the Norwood surgery using multi-domain modeling,” *J. Biomech. Eng.*, vol. 134, no. 5, p. 51002, 2012.

[6] M. Esmaily-Moghadam, B. Murtuza, T.-Y. Hsia, and A. Marsden, “Simulations reveal adverse hemodynamics in patients with multiple systemic to pulmonary shunts,” *J. Biomech. Eng.*, vol. 137, no. 3, p. 31001, 2015.

[7] F. Migliavacca *et al.*, “Modeling of the Norwood circulation: effects of shunt size, vascular resistances, and heart rate,” *Am. J. Physiol. Circ. Physiol.*, vol. 280, no. 5, pp. H2076--H2086, 2001.

[8] O. Petrucci, P. R. Khoury, P. B. Manning, and P. Eghtesady, “Outcomes of the bidirectional Glenn procedure in patients less than 3 months of age,” *J. Thorac. Cardiovasc. Surg.*, vol. 139, no. 3, pp. 562–568, 2010.

[9] R. D. B. Jaquiss *et al.*, “Early cavopulmonary anastomosis in very young infants after the Norwood procedure: impact on oxygenation, resource utilization, and mortality,” *J. Thorac. Cardiovasc. Surg.*, vol. 127, no. 4, pp. 982–989, 2004.

[10] D. di Carlo, W. G. Williams, R. M. Freedom, G. A. Trusler, and R. D. Rowe, “The role of cava-pulmonary (Glenn) anastomosis in the palliative treatment of congenital heart disease,” *J. Thorac. Cardiovasc. Surg.*, vol. 83, no. 3, pp. 437–442, 1982.

[11] M. Esmaily Moghadam, T.-Y. Hsia, A. L. Marsden, M. of Congenital Hearts Alliance (MOCHA) Investigators, and others, “The assisted bidirectional Glenn: A novel surgical approach for first-stage single-ventricle heart palliation,” *J. Thorac. Cardiovasc. Surg.*, vol. 149, no. 3, pp. 699–705, 2015.

[12] F. Gervaso, S. Kull, G. Pennati, F. Migliavacca, G. Dubini, and V. S. Luisi, “The effect of the position of an additional systemic-to-pulmonary shunt on the fluid dynamics of the bidirectional cavo-pulmonary anastomosis.,” *Cardiol. Young*, vol. 14, 2004.

[13] J. Zhou *et al.*, “In vitro assessment of the assisted bidirectional Glenn procedure for

stage one single ventricle repair," *Cardiovasc. Eng. Technol.*, vol. 6, no. 3, pp. 256–267, 2015.

[14] J. K. Shang *et al.*, "Patient-specific multiscale modeling of the assisted bidirectional Glenn," *Ann. Thorac. Surg.*, vol. 107, no. 4, pp. 1232–1239, 2019.

[15] A. Verma *et al.*, "Optimization of the assisted bidirectional Glenn procedure for first stage single ventricle repair," *World J. Pediatr. Congenit. Hear. Surg.*, vol. 9, no. 2, pp. 157–170, 2018.

[16] W. M. DeCampli, "The steam locomotive makes a comeback: A new solution to staged single-ventricle palliation?," *J. Thorac. Cardiovasc. Surg.*, vol. 149, no. 3, pp. 706–707, 2015.

[17] C. D. Morgan, M. S. Wolf, T. M. Le, C. N. Shannon, J. C. Wellons, and B. A. Mettler, "Cerebral ventriculomegaly after the bidirectional Glenn (BDG) shunt: a single-institution retrospective analysis," *Child's Nerv. Syst.*, vol. 31, no. 11, pp. 2131–2134, 2015.

[18] J. F. Lea, H. V. Nickens, and M. R. Wells, *Gas Well Deliquification*. 2008.

[19] M. E. Moghadam, I. E. Vignon-Clementel, R. Figliola, A. L. Marsden, M. of Congenital Hearts Alliance (MOCHA) Investigators, and others, "A modular numerical method for implicit 0D/3D coupling in cardiovascular finite element simulations," *J. Comput. Phys.*, vol. 244, pp. 63–79, 2013.

[20] M. Esmaily-Moghadam, Y. Bazilevs, and A. L. Marsden, "A bi-partitioned iterative algorithm for solving linear systems arising from incompressible flow problems," *Comput. Methods Appl. Mech. Eng.*, vol. 286, pp. 40–62, 2015.

[21] M. Esmaily-Moghadam, Y. Bazilevs, and A. L. Marsden, "A new preconditioning technique for implicitly coupled multidomain simulations with applications to hemodynamics," *Comput. Mech.*, vol. 52, no. 5, pp. 1141–1152, 2013.

[22] P. Ladeveze and D. Leguillon, "Error estimate procedure in the finite element method and applications," *SIAM J. Numer. Anal.*, vol. 20, no. 3, pp. 485–509, 1983.

[23] P. Luchini, "An adaptive-mesh finite-difference solution method for the Navier-Stokes equations," *J. Comput. Phys.*, 1987, doi: 10.1016/0021-9991(87)90059-3.

[24] P. MOSHER, J. ROSS, P. A. MCFATE, and R. F. SHAW, "CONTROL OF CORONARY BLOOD FLOW BY AN AUTOREGULATORY MECHANISM.," *Circ. Res.*, 1964, doi: 10.1161/01.RES.14.3.250.

[25] H. Si, "TetGen, a delaunay-based quality tetrahedral mesh generator," *ACM Trans. Math. Softw.*, 2015, doi: 10.1145/2629697.

[26] D. E. Rivera, M. Morarl, and S. Skogestad, "Internal Model Control: Pid Controller Design," *Ind. Eng. Chem. Process Des. Dev.*, 1986, doi: 10.1021/i200032a041.

[27] J. G. Ziegler and N. B. Nichols, "Optimum settings for automatic controllers," *J. Dyn. Syst. Meas. Control. Trans. ASME*, 1993, doi: 10.1115/1.2899060.

[28] A. L. Marsden and M. Esmaily-Moghadam, “Multiscale modeling of cardiovascular flows for clinical decision support,” *Appl. Mech. Rev.*, vol. 67, no. 3, p. 30804, 2015.

[29] F. M. A. Box, R. J. van der Geest, M. C. M. Rutten, and J. H. C. Reiber, “The influence of flow, vessel diameter, and non-Newtonian blood viscosity on the wall shear stress in a carotid bifurcation model for unsteady flow,” *Invest. Radiol.*, vol. 40, no. 5, pp. 277–294, 2005.

[30] M. E. Moghadam, Y. Bazilevs, T.-Y. Hsia, I. E. Vignon-Clementel, A. L. Marsden, and others, “A comparison of outlet boundary treatments for prevention of backflow divergence with relevance to blood flow simulations,” *Comput. Mech.*, vol. 48, no. 3, pp. 277–291, 2011.

[31] J. Caspi, T. W. Pettitt, T. Mulder, and A. Stopa, “Development of the pulmonary arteries after the Norwood procedure: comparison between Blalock-Taussig shunt and right ventricular--pulmonary artery conduit,” *Ann. Thorac. Surg.*, vol. 86, no. 4, pp. 1299–1304, 2008.

[32] M. Griselli *et al.*, “Fate of pulmonary arteries following Norwood procedure,” *Eur. J. cardio-thoracic Surg.*, vol. 30, no. 6, pp. 930–935, 2006.

[33] J. D. Pruetz, S. Badran, F. Dorey, V. A. Starnes, and A. B. Lewis, “Differential branch pulmonary artery growth after the Norwood procedure with right ventricle--pulmonary artery conduit versus modified Blalock--Taussig shunt in hypoplastic left heart syndrome,” *J. Thorac. Cardiovasc. Surg.*, vol. 137, no. 6, pp. 1342–1348, 2009.

[34] G. S. Kopf, H. Laks, H. C. Stansel, W. E. Hellenbrand, C. S. Kleinman, and N. S. Talner, “Thirty-year follow-up of superior vena cava-pulmonary artery (Glenn) shunts,” *J. Thorac. Cardiovasc. Surg.*, vol. 100, no. 5, pp. 662–671, 1990.

[35] A. L. Marsden *et al.*, “Evaluation of a novel Y-shaped extracardiac Fontan baffle using computational fluid dynamics,” *J. Thorac. Cardiovasc. Surg.*, vol. 137, no. 2, pp. 394–403, 2009.

[36] W. Yang, I. E. Vignon-Clementel, G. Troianowski, V. M. Reddy, J. A. Feinstein, and A. L. Marsden, “Hepatic blood flow distribution and performance in conventional and novel Y-graft Fontan geometries: a case series computational fluid dynamics study,” *J. Thorac. Cardiovasc. Surg.*, vol. 143, no. 5, pp. 1086–1097, 2012.

[37] C. M. Haggerty *et al.*, “Simulating hemodynamics of the Fontan Y-graft based on patient-specific in vivo connections,” *J. Thorac. Cardiovasc. Surg.*, vol. 145, no. 3, pp. 663–670, 2013.

[38] M. H. Martin, J. A. Feinstein, F. P. Chan, A. L. Marsden, W. Yang, and V. M. Reddy, “Technical feasibility and intermediate outcomes of using a handcrafted, area-preserving, bifurcated Y-graft modification of the Fontan procedure,” *J. Thorac. Cardiovasc. Surg.*, vol. 149, no. 1, pp. 239–245, 2015.

[39] L. B. Leverett, J. D. Hellums, C. P. Alfrey, and E. C. Lynch, “Red blood cell damage by shear stress,” *Biophys. J.*, vol. 12, no. 3, pp. 257–273, 1972.

[40] K. Vahidkhah *et al.*, “Flow-induced damage to blood cells in aortic valve stenosis,”

Ann. Biomed. Eng., vol. 44, no. 9, pp. 2724–2736, 2016.

[41] W.-T. Wu, M. A. Jamiolkowski, W. R. Wagner, N. Aubry, M. Massoudi, and J. F. Antaki, "Multi-constituent simulation of thrombus deposition," *Sci. Rep.*, vol. 7, p. 42720, 2017.

[42] C. C. Long, M.-C. Hsu, Y. Bazilevs, J. A. Feinstein, and A. L. Marsden, "Fluid--structure interaction simulations of the Fontan procedure using variable wall properties," *Int. j. numer. method. biomed. eng.*, vol. 28, no. 5, pp. 513–527, 2012.

[43] D. Tamisier, P. R. Vouhé, F. Vernant, F. Leca, C. Massot, and J. Y. Neveux, "Modified Blalock-Taussig shunts: Results in infants less than 3 months of age," *Ann. Thorac. Surg.*, 1990, doi: 10.1016/0003-4975(90)90026-3.

[44] N. A. Guzzetta, G. S. Foster, N. Mruthinti, P. D. Kilgore, B. E. Miller, and K. R. Kanter, "In-hospital shunt occlusion in infants undergoing a modified blalock-taussig shunt," *Ann. Thorac. Surg.*, 2013, doi: 10.1016/j.athoracsur.2013.03.026.